Frequenz
63 (2009)
1–2

A Compact Ultra-wideband Radar for Medical Applications

Mario Leib, Eva Schmitt, Arnold Gronau, Jochen Dederer, Bernd Schleicher, Hermann Schumacher and Wolfgang Menzel

Abstract – In this article an impulse based radar system operating in the ultra-wideband frequency range between 3.1 GHz and 10.6 GHz is presented. The radar sensor is intended to be used in medical diagnostics. In principle the realized radar could be applied to various applications, especially due to the compact overall size and the size of the radar front-ends in particular. One focus of the paper is on a detailed description of the system architecture with the correlation receiver and the time delay adjustment using a variable phase setting for the trigger signals. Furthermore, the key components of the radar, the monolithically integrated pulse generator and the planar antenna, are explained. The capabilities of the radar and the correlation principle are shown in different validation measurements, where a metal plate is used as an ideal target. In addition, two different methods for movement detection were demonstrated successfully measuring the respiration and the heart beat of a test person.

Index Terms – pulse radar, ultra-wideband, correlation receiver, medical diagnosis

1. Introduction

In general, the Ultra-wideband (UWB) technology has a very long history. When in 1886 Heinrich Hertz transmitted electromagnetic signals from a transmitter to a receiver, he unintentionally used already very broadband pulse signals [1]. Since then, narrowband systems were preferred due to their better interoperability. Nowadays, the UWB technology is gaining new interest. First it has been exploited mainly by the military, but since the Federal Communication Commission (FCC) in 2002 approved the regulations for the general use of UWB in the USA, research on UWB systems started for civilian applications as well; in particular in the frequency range from 3.1 – 10.6 GHz. The power density limitations within this frequency band, with a maximum allowed EIRP of -41.3 dBm/MHz (see [2]), ensure that UWB systems can coexist with narrowband systems. In Europe the bandwidth for generic admission of ultra-wideband systems with this power density is reduced to 6.0 – 8.5 GHz by the Electronic Communications Committee (ECC) [3]. Due to the low transmit power, only short-range UWB systems are feasible. However, high-resolution sensing and high-data rate communication can be realized because of the wide bandwidth.

For radar sensors the possible simple transceiver architecture and low-power consumption are further advantages leading to different civilian applications like wall scanners [4], detection of buried people [5], intrusion sensors [6], positioning systems [7], material characterization [8], tank level sensors [9], et cetera. Beside these applications, UWB radar systems are of particular interest in the area of medical technology due to the non-ionizing radiation (compared to X-rays) and the low probability of interference with other technical equipment [10]. One major target application is the detection of breast cancer. This can be achieved with an UWB imaging system based on a significant difference in the permittivity of breast tissue and malignant breast tumors. This application is still a current research topic, and up to now only simulations [11] or measurements with phantom tissues [12] have been performed. Another emerging medical application is the contact-free measurement of vital signals (respiration and heart beat) of human beings [13, 14]. This could be of interest for convenient remote monitoring of patients, e.g. burned victims, where attachment of sensors is impossible in the affected body areas. In contrast to a Doppler radar [15], such a UWB radar sensor could also be used to monitor the actual position of organs during a computer tomography (CT) using range gating. This could be applied to compensate the organ movement in the CT post-processing leading to an improved image. Furthermore, thorax excursion measurements could be performed for medical research to detect pathological breathing patterns in intensive care settings.

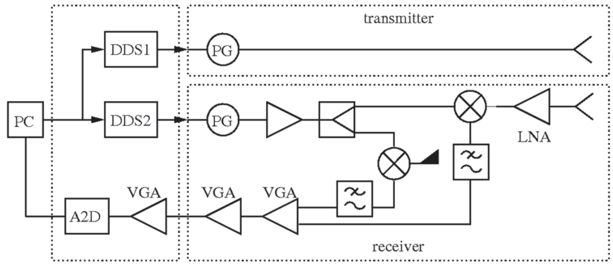

Fig. 1: Block diagram of the bistatic UWB radar.

In this publication, a single-channel UWB radar sensor operating in the frequency range of 3.1 GHz – 10.6 GHz will be presented in detail. The radar sensor can be applied to all afore mentioned applications in the medical environment. In this contribution the focus is on the capabilities for high resolution imaging and vital signal detection. The bandwidth according to the FCC regulations instead of the ECC is chosen due to the improved resolution performance.

2. System Concept

The basic sensor concept is a pulse radar with very short transmitted pulses in order to achieve a high resolution. The transmitter consists of only a pulse generator and an antenna. A correlation principle is applied for the receiver [14]. The necessary delay for the correlation is adjusted with a variable phase setting of the trigger signal for the pulse generator instead of using a mandatory broadband, widely tunable and precise true time delay, which would be hard to realize. In summary this results in a simple architecture that can operate at low power and has low production cost. A bistatic setup has been chosen to be able to apply the sensor to many different test scenarios and to avoid a duplexer or a transmit/receive switch.

2.1 System Architecture

In Fig. 1 the detailed block diagram of the realized single-channel, bistatic UWB radar is depicted. The only basic blocks of the transmitter are the pulse generator (PG) and the antenna. In the receiver, the incoming signal is amplified by a broadband, low-noise amplifier (LNA) and then multiplied with the signal of a reference pulse generator. The correlator in the receiver is formed by the reference signal generator with an adjustable trigger signal, the multiplier and an integrator. If the reference signal of the correlator is equal to the received signal, the correlation concept is equal to a matched filter maximizing the signal-to-noise ratio (SNR). Due to the poor IF-LO isolation of the commercial mixer a symmetrical arrangement with two identical correlator branches has been used, where one branch is connected to a load and one to the antenna with the receiving signal. Combining both signal paths with a differential amplifier leads to a suppression of the parasitic LO leakage signal at the output of the differential amplifier.

2.2 Time Delay Adjustment

In the previously described architecture, a phase shift of the trigger signal for the two pulse generators is equivalent to a time delay at the output of the pulse generators as illustrated in Fig. 2. As long as the period of the trigger signal is larger than the propagation delay of the received signal, the unambiguous time delay of the received signal can be obtained. When the time delay (phase shift) of the reference pulse generator is equal to the propagation delay of the received signal, the maximum signal amplitude will occur at the output of the correlator. The distance of a target is then proportional to the trigger signal phase shift. If the time delay (phase) is shifted in small time increments over the observation range, the correlation function of the reference and received signal will be captured.

The necessary phase shift can be obtained either by an analog phase shifter or digitally, e. g., by the use of a direct digital synthesizer (DDS). In our approach a DDS has been used, as the trigger frequency of the two DDS can be synchronized and adjusted easily. As a result, the radar can be applied to different application scenarios in a very flexible manner. Varying the detection distance, however, is relatively slow as programming of the phase shift for the DDS takes some time. Nevertheless, an adjustment to a certain range is possible, which can be applied to measure fine movement variations, as will be shown later on.

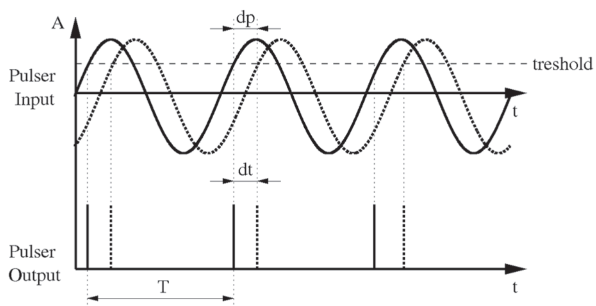

Fig. 2: Time delay generation using a phase shift for the trigger signal.

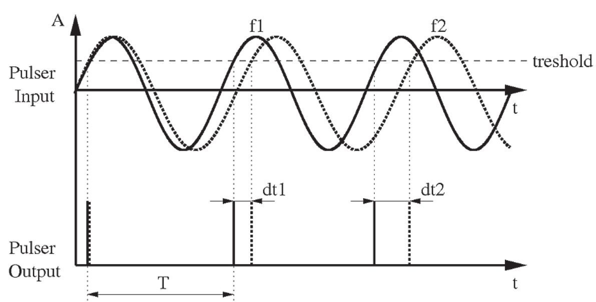

Fig. 3: Time delay adjustment using different trigger frequencies.

In order to achieve a continuous monitoring of the target distance, an alternative method can be applied. If a small frequency offset is provided between the trigger signals for the transmitter and the reference pulse generator, an increasing phase difference between the trigger signals and, therefore, an increasing time delay for the reference pulse generators will occur (see Fig. 3). In this way, the time delay is changed continuously. The time difference between equal phase states and the occurrence of a correlation signal at the output is proportional to the target distance [16]. Therewith, a fast scanning of a certain range in front of the radar can be achieved. With a sufficiently high trigger signal frequency, a nearly real-time display is possible.

3. Key Components

The key components of the radar system are the pulse generator and the antenna, which will be introduced in the following sections. For the other parts, commercially available components have been used. Although for the LNA and the multiplier no building blocks specified up to 10.6 GHz were available, an amplifier and a mixer with acceptable results could be found based on the characterization of several different components. For the next generation of this radar sensor, these components will be replaced by custom-designed monolithically integrated circuits [17]. An improvement of the overall system performance is expected then.

3.1 Pulse Generator

The operation principle of the pulse generator can be divided into three sub-circuits [18]. The first part is fed by the trigger signal and converts this input signal from a potentially large rise-time signal into a rectangular signal with a very short rise time. In the second sub-circuit, this signal is differentiated, and the corresponding negative slope of the rectangular signal is suppressed resulting in an output signal similar to a Gaussian bell shape with a small width. Finally, the third sub-circuit acts as a monocycle pulse shaper generating the first derivative of the Gaussian input pulse. The measured output signal of an assembled pulse generator showing this pulse shape can be seen in Fig. 4. The monolithically integrated circuit (IC) was fabricated in a low-cost 0.8 µm-Si/SiGe HBT technology. Its dimensions are 560 µm x 560 µm. More details about the circuit design and more measurement results can be found in [18].

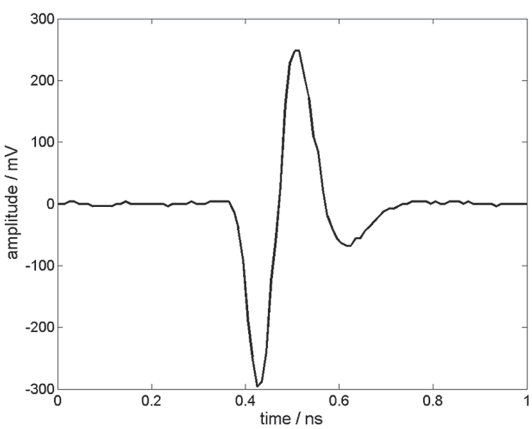

Fig. 4: Measured output signal of the pulse generator.

Frequenz 63 (2009) 1–2

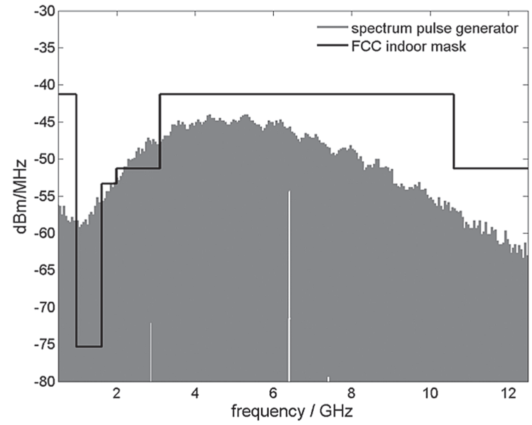

Fig 5: Measured spectrum of the pulse generator.

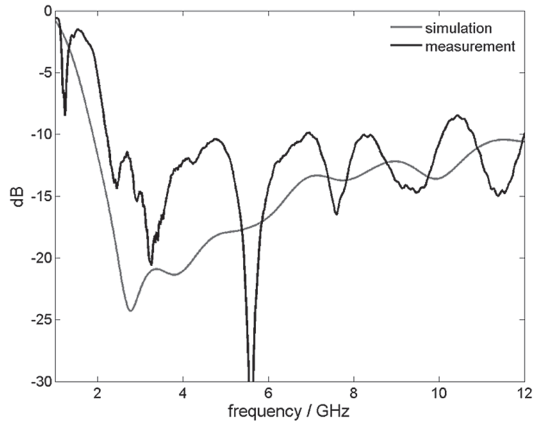

Fig. 7: Simulated and measured reflection coefficient for the Vivaldi antenna.

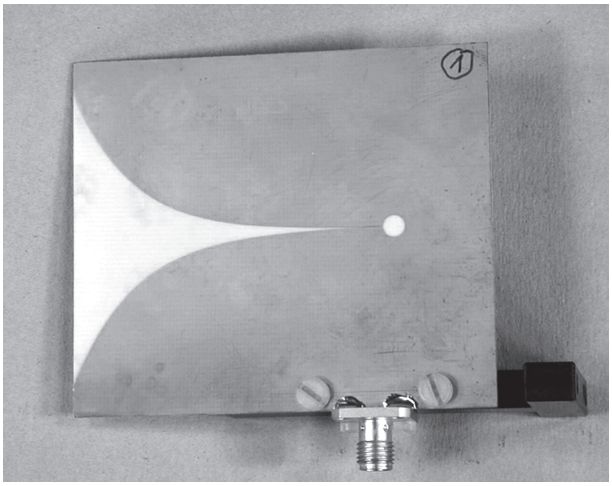

Fig. 6: Photograph of the Vivaldi antenna including an SMA connector for characterization purposes.

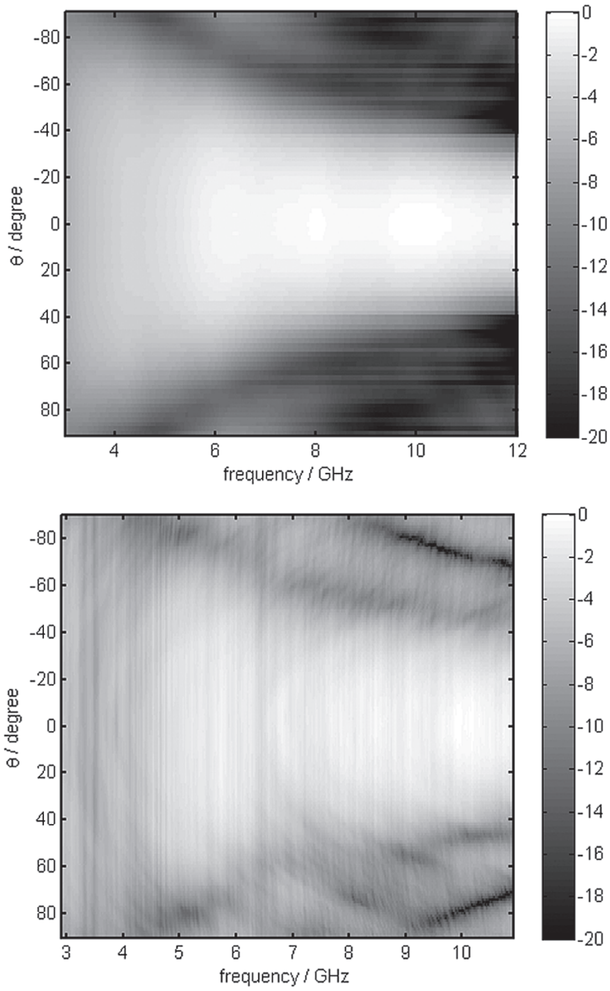

Fig. 8: Simulated (top) and measured (bottom) normalized gain of the Vivaldi antenna in dB (H-Plane, Co-Polarization).

The spectrum of the output signal for a trigger repetition frequency of 30 MHz is shown in Fig. 5, including also the FCC UWB frequency mask for indoor applications. As can be seen the spectrum fits well into this mask for high frequencies, but violates the mask for lower frequencies. In order to achieve an FCC compliant spectrum, the 5^{th} derivative of a Gaussian bell shape has to be generated at the output of the pulse generator [17]. For an ECC compliant radar system with a reduced resolution capability, a pulse generator with a bandwidth of 6–8.5 GHz needs to be realized.

3.2 Vivaldi Antenna

For the transmitter and the receiver, the well-known Vivaldi antenna [19] has been chosen because of the directive behavior, linear polarisation, moderate size, and planar realization. A Vivaldi antenna is a travelling wave antenna with an exponentially tapered slot line (see Fig. 6). Therefore, this antenna type has a very broadband behavior. A microstrip line is used for the external antenna port to be able to apply easily an SMA connector for the antenna characterization and to integrate the ICs directly on the antenna for a compact sensor. The transition from the slotline is achieved using a planar Marchand balun with circular open circuits in microstrip and slot line [20]. On the used substrate (RO4003) with a substrate height of 0.5 mm, a return loss of more than 10 dB is obtained in the frequency range from 2.4 GHz to 10.6 GHz (see Fig. 7). Compared to the simulation results, the matching performance is deteriorated. Further simulations showed that the SMA connector is responsible for the ripples in the reflection coefficient curve. For the sensor with the transmit and receive circuits integrated on the antenna substrate, a matching behavior similar to the simulated results is expected.

The main radiation direction of the antenna is in the direction of the tapered slot, but the radiation characteristic is varying for different angles and frequencies. Exemplarily, the radiation pattern for the interesting frequency range and the H-plane (perpendicular to the substrate) is depicted in Fig. 8 for the simulated and measured results. In both cases, the

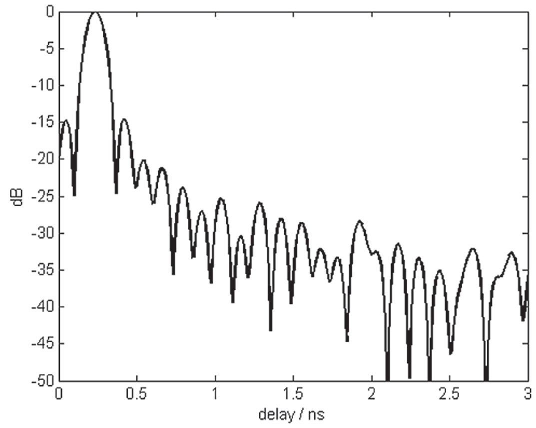

Fig. 9: Normalized envelope of the impulse response for the Vivaldi antenna in the main radiation direction (Co-Polarization).

antenna gain is normalized to the determined maximum gain of 9.3 dBi. In general, a good agreement between measurement and simulation is achieved. For the measured results, a slight decrease of gain at lower frequencies and higher side lobes is obtained.

Since the propagation velocity in the slotline of the antenna is quite constant over frequency, the antenna is well suited for impulse radiation. This can be demonstrated observing the time domain behavior of the antenna. The antenna's impulse response is calculated from the amplitude and phase information in frequency domain using the inverse Fourier transformation, a Kaiser window and zero padding (for a fine time resolution) [21]. The envelope of the resulting and normalized impulse response for the measured data is presented in Fig. 9 for the case of radiation in direction of the main antenna beam. As can be seen, the secondary maxima of the impulse response are suppressed by more than 14 dB showing the good ringing performance of the antenna. Furthermore, the full width of the pulse envelope at half maximum (FWHM) has a very small value of 110 ps indicating the low dispersion behavior of the antenna. Similar impulse responses are obtained for other radiation angles.

4. Realized UWB Radar System

Transmitter and receiver of this bistatic radar have been integrated each on the respective antenna substrate in hybrid circuit technology to avoid multiple reflections due to external connectors. Both modules are mounted within a metallic housing, where the housings can be connected together achieving nearly a monostatic setup (see Fig. 10). However, in this case, a strong direct coupling from the transmitter to the receiver can be discovered resulting in a ghost target at a very short distance. This ghost target can be removed with a reference measurement without any targets and a subtraction of this response from a measured response.

Additional power supply circuitry is implemented on the two radar modules (1), so that the complete front-end can be operated from a single supply voltage. Power supply and all other supplementary functions are provided by a synchronous control and measurement electronic unit (2). This box includes the DDS for the trigger signals and their programming for synchronization and time control, the analog-to-digital conversion, further amplification, and controlling of the data transfer via an USB interface to a PC. It has originally been developed for the use in an FMCW radar system [22] and therefore has more features than actually needed for this application. With a specific development for this UWB radar, an even more compact electronic circuitry with less power

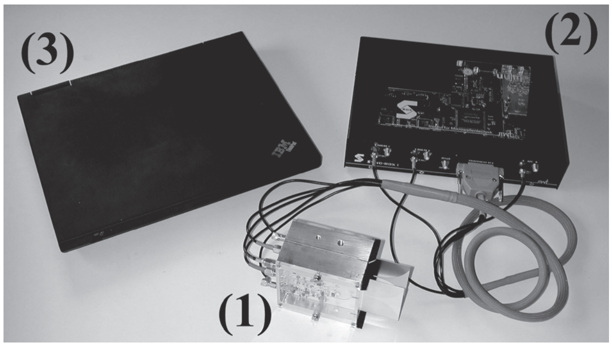

Fig. 10: Photograph of the complete UWB radar sensor system with radar modules (1), electronic unit (2), and notebook (3).

consumption could be realized. Nevertheless, combined with a notebook (3), the complete sensor system is already quite compact, as can be seen in Fig. 10. Therefore, it is easily applicable to different measurement scenarios, as will be described in the next section.

5. Measurement Results

With the previously described system first validation tests have been performed. These measurement results will be presented next, and afterwards some results concerning possible medical scenarios will be shown.

5.1 Radar Sensor Validation

In a first experiment a metal plate, representing an ideal target, has been positioned in front of the UWB radar in order to demonstrate the general operation of the sensor. In Fig. 11 the measured output of the UWB radar is displayed for different target distances, where the phase between the two trigger signals has been adjusted in fine steps. There, the clearly visible correlation function is obtained for each target distance and the maximum value of the expected correlation function corresponds to the position of the metal plate. The amplitude of the measured response is decreasing with distance. It can be shown that the amplitude decrease is inversely proportional to the target distance R. This is valid as the large metal plate acts as an ideal reflector for small distances leading to a condition like in communication systems, when the transmitter and the receiver are separated by the distance R. The difference between the actual and the measured target position in Fig. 11 is caused by the fact that the transmitter and the receiver were separated laterally by

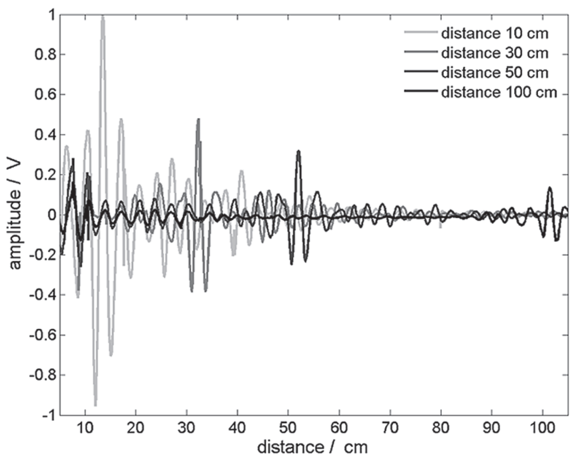

Fig. 11: Radar sensor output for different target positions.

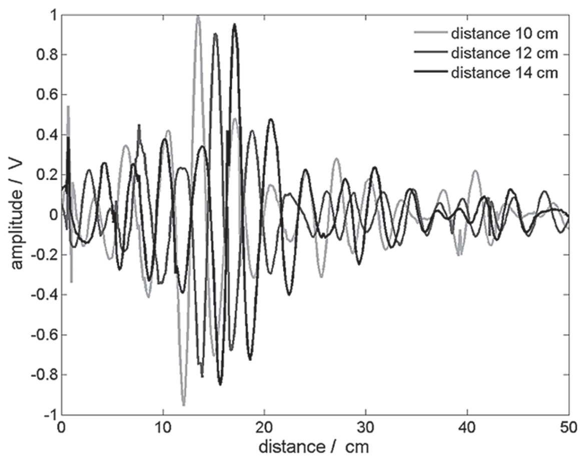

Fig. 12: Sensor output for small target positions variations.

about 20 cm to reduce the antenna coupling. Furthermore, the system has not been calibrated at this early stage of testing, and therefore the time delay within the receiver causes an additional offset in the absolute target position. Due to the size limitations in the laboratory, results could be recorded only up to 2.5 m. In a next test, the target position was changed in steps of only 2 cm.
As can be seen in Fig. 12, these varying target positions are still clearly distinguishable and the difference between the maximum values is also about 2 cm.

Beside the mode described above, where the phase between the pulse generators is shifted consecutively, the frequency offset mode has also been applied to the radar system. To demonstrate the ability for the detection of slow movements, a metal plate was placed in front of the radar moving slowly back and forth by 6.5 cm with 0.3 Hz. This movement could be visualized on a PC monitor with a small time delay.

With this mode, slow movements in relation to the monitor update rate can be observed. The update rate is mainly determined by the time duration of a range scan, which is inversely proportional to the frequency offset Δf between the trigger frequencies.

A tradeoff between scanning time and integration has to be made. For the previously described measurement, a scanning time of 200 ms and an integration filter with 100 Hz bandwidth is used leading to a sufficiently small signal-to-noise ratio and a maximum update rate of 5 Hz for the observed range of 0.5 m.

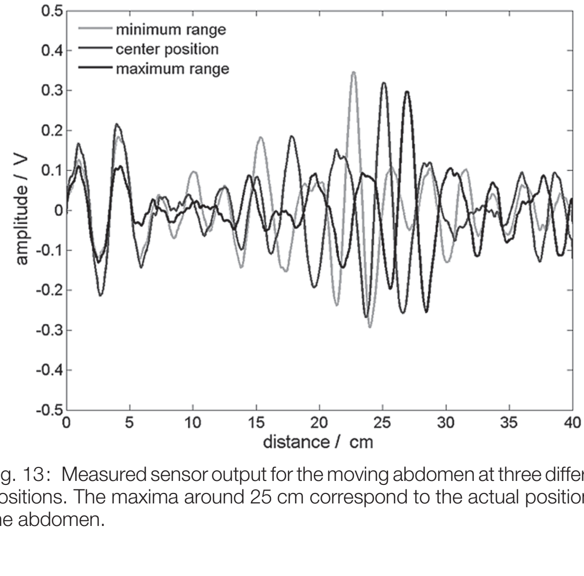

Fig. 13: Measured sensor output for the moving abdomen at three different positions. The maxima around 25 cm correspond to the actual position of the abdomen.

5.2 Test Measurements for Medical Applications

As already mentioned in the previous section, movements can be detected using the mode with two slightly different trigger frequencies, where the area in front of the radar is scanned continuously. But the visualization of a moving target is only possible, if the range scanning time is several times faster than the change of the target position. This condition is met for the breathing of a human being. In order to measure the breathing rate, the radar sensor was directed towards the abdomen of a test person.
At the abdominal wall a maximum range variation is expected. In Fig. 13 the radar response for three different positions (minimum, center, maximum) for the abdominal wall are shown. The detected reflected wave is caused by the strong permittivity difference between human tissue and air. Compared to the measurements with a metal plate, the amplitude of the received signal is significantly lower due to the fact that the radiated electromagnetic wave is partially penetrating into and mainly absorbed within the human body. The overall movement range of the abdominal wall can be observed easily. In this case 4.3 cm were obtained due to a deep breathing of the test person. This information is valuable for the analysis of the respiration behavior of a person or for thorax excursions measurements and gained already some interest by physicians. In principle, with the timing information of the sensor, the breathing rate could be calculated. Another method with an easier feasibility compared to this realization will be explained in the following.

Instead of measuring the breathing rate by scanning the range in front of the radar continuously, the target movement within a small range can be detected with this sensor by fixing the range to the position of the target (maximum of the correlation function). If the target then moves back or forth, the amplitude will decrease as far as the local position change is within a small range around the maximum of the correlation function. Then, the output signal of the sensor shows the position variation over time.

When the sensor is directed towards the abdomen or the breast of a person with fixed range adjustment, the breathing of a person results in a periodic output signal of the sensor. In Fig. 14a the result of such a measurement is presented. The radar is directed towards the sternum and placed 10 cm in front of the person. In this example, the person is breathing deeply during the first 15 s, stops breathing for a while and starts breathing again. If a Fourier transformation is applied to the first 15 s of the sensor signal, the person's breathing rate of 0.27 Hz (16.2 breaths/min) can be obtained determining the maximum value of the spectrum (see Fig. 14b). The first peak around 0.03 Hz is caused by slow movement of the upper part of the body while the person is standing. This possible error source can be suppressed with additional filtering.

If the time span without breathing (16 s – 24 s) is observed more closely and some smoothing is applied, then the signal displayed in Fig. 14c is obtained. This, once again, periodic signal shows the heart beat of the person. With a Fourier transformation the heart rate can be determined easily (see Fig. 14d). In this case, a typical heart beat rate of 69.6 beats per minute (1.16 Hz) is measured. In the setup, the range gate is fixed to the boundary between the human body and air. The heart beat is actually recognizable, as shock waves created by the heart cause a movement of the outer skin area.

For more corpulent persons, compared to the quite slim test person, this signal may not be observable anymore. So, more verification measurements with persons of different physique have to be performed. In principle, it should be possible to detect the heart beat directly, if the range gate is fixed to the cardiac wall, because a significant permittivity difference between the heart muscle (ε_r of approx. 50) and the surrounding tissue (fat, ε_r of approx. 5) exists. The signal reflected at

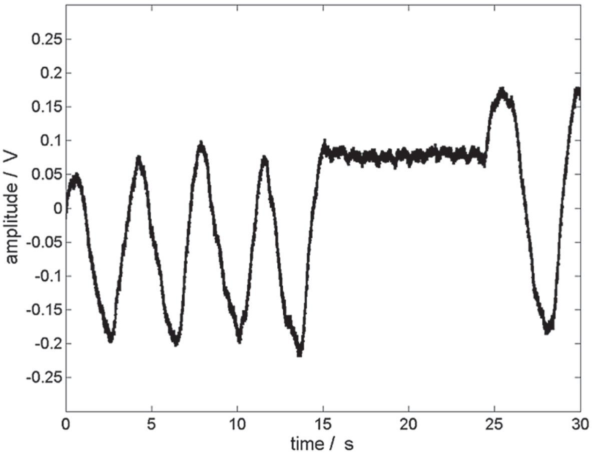

Fig. 14a: Measured signal of the sensor directed towards a breathing person with different breathing behavior.

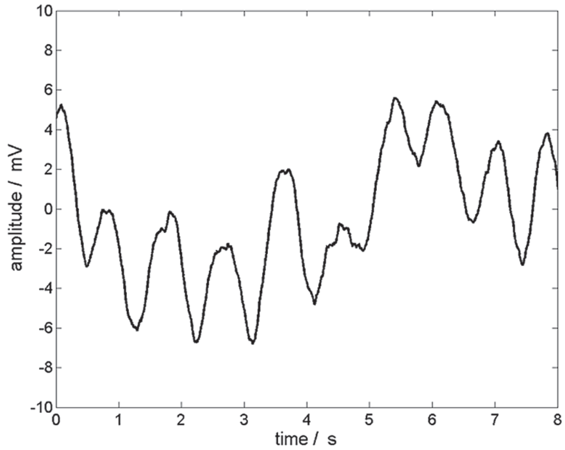

Fig. 14c: Measured and smoothed signal, when the radar sensor is directed towards a person suppressing breathing (compare Fig. 14a).

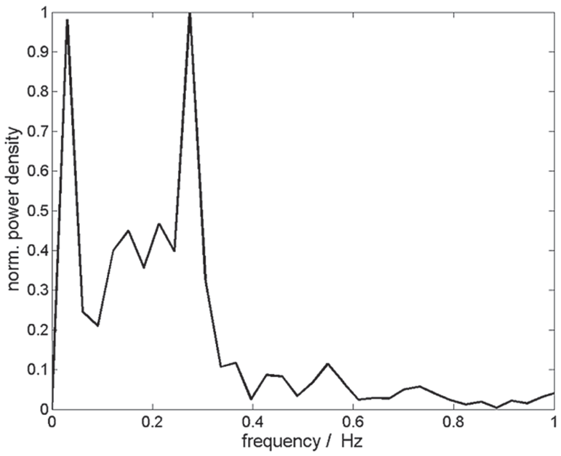

Fig. 14b: Fourier transformation of the signal in Fig. 14a, when the test person is breathing.

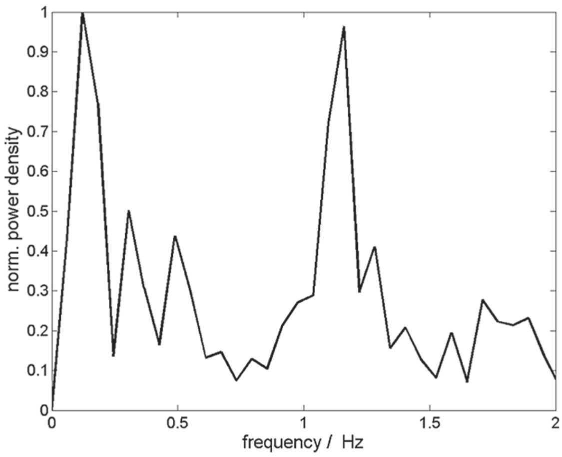

Fig. 14d: Fourier transformation for the measured heart beat signal of a person displayed in Fig. 14c.

this discontinuity inside the human body is highly attenuated and therefore more challenging for detection.

6. Conclusion

The presented compact UWB radar sensor with its simple architecture is applied successfully for the measurement of vital signals (respiration and heart beat) and the thorax excursion of a human being in a laboratory environment.
Further potential applications in the field of medical diagnostics for this sensor are detection of organ movement, and, in case of a sensor array, localization of interventional devices. These fields will be addressed in the future, but are challenging due to the high losses and dispersive effects within the human body. In a next step an improved setup with custom-designed SiGe ICs and an increased performance is planned. Furthermore, an improvement of the target resolution with an advanced signal processing technique using a Wiener filter is intended.

7. References

[1] H. Schantz, The Art and Science of Ultra-Wideband Antennas. Norwood, USA: Artech House, 2005.
[2] Federal Communications Commission, "Revision of part 15 of the commission's rules regarding ultra-wideband transmission systems", Washington D.C., USA, First Report & Order 48–02, Apr. 2002.
[3] Electronic Communications Committee, "ECC decision of 24 March 2006 on the harmonised conditions for devices using ultra-wideband (UWB) technology in bands below 10.6 GHz", Mar. 2006.
[4] S. Hantscher, A. Reisenzahn, and C. G. Diskus, "An UWB wall scanner based on a shape estimating SAR algorithm", IEEE Int. Symp. on Microwave Theory and Techniques, Jun. 2007, pp. 1463–1466.
[5] E. Zaikov, J. Sachs, M. Aftanas, and J. Rovnakova, "Detection of trapped people by UWB radar", German Microwave Conf., Mar. 2008, pp. 240–243.
[6] I. Immoreev, P. G. Samkov, and T. Tao, "Short-distance ultra-wideband radars. Theory and designing", Int. Conf. on Radar Systems, Oct. 2004.
[7] R. J. Fontana, "Recent system applications of short-pulse ultra-wideband (UWB) technology", IEEE Trans. on Microwave Theory and Techniques, vol. 52, no. 9, pp. 2087–2104, Sep. 2004.
[8] A. Gülck and R. Knöchel, "Three-dimensional position estimation of dielectric objects using UWB-pulses and cross-correlation", German Microwave Conf., Mar. 2008, pp. 252–255.
[9] T. McEwan and S. Azevedo, "Micropower impulse radar", Science & Technology Review, Jan. 1996.
[10] C. G. Bilich, "Bio-medical sensing using ultra-wideband communications and radar technology: A feasibility study", Int. Conf. on Pervasive Computing Technologies for Healthcare, Oct. 2006.
[11] S. K. Davis, B. D. V. Veen, S. C. Hagness, and F. Kelcz, "Breast tumor characterization based on ultrawideband microwave backscatter", IEEE Trans. on Biomedical Engin., vol. 55, no. 1, pp. 237–246, Jan. 2008.

[12] M. Klemm, I.J. Craddock, J. Leendertz, A. W. Preece, and R. Benjamin, "Breast cancer detection using symmetrical antenna array", European Conf. on Antennas and Propagation, Nov. 2007.
[13] E. M. Staderini, "UWB radars in medicine", IEEE Aerospace and Electronic Systems Mag., vol. 17, no. 1, pp. 13–18, Jan. 2002.
[14] M. Chia, S. Leong, C. Sim, and K. Chan, "Through-wall UWB radar operating within FCC's mask for sensing heart beat and breathing rate", European Radar Conf., Oct. 2005, pp. 267–270.
[15] M. Jelen and E. M. Biebl, "Multi-frequency sensor for remote measurement of breath and heartbeat", Advances in Radio Science, vol. 4, pp. 79–83, 2006.
[16] J. Motzer, "A pulse radar gauge for level measurement and process control", in IEEE Int. Symp. on Microwave Theory and Techniques, vol. 3, June 2000, pp. 1563–1566.
[17] J. Dederer, B. Schleicher, F. A. T. Santos, A. Trasser, and H. Schumacher, "FCC compliant 3.1–10.6 GHz UWB pulse radar using correlation detection", IEEE Int. Symp. on Microwave Theory and Techniques, Jun. 2007, pp. 1471–1474.
[18] J. Dederer, C. Schick, A. Trasser, and H. Schumacher, "A SiGe impulse generator for single-band ultra-wideband applications", Semiconductor Science and Technology, vol. 22, no. 1, Jan. 2007, pp. 200–203.
[19] W. Sörgel, C. Waldschmidt, and W. Wiesbeck, "Transient responses of a Vivaldi antenna and a logarithmic periodic dipole array for ultra wideband communication", IEEE Int. Symp. on Antennas and Propagation, vol. 3, Jun. 2003, pp. 592–595.
[20] B. Schüppert, "Microstrip/slotline transitions: Modeling and experimental investigation", IEEE Trans. on Microwave Theory and Techniques, vol. 36, no. 8, pp. 1272–1282, Aug. 1988.
[21] W. Sörgel and W. Wiesbeck, "Influence of the antennas on the ultra-wideband transmission", EURASIP Journal on Applied Signal Processing, vol. 2005, no. 3, pp. 296–305, 2005.
[22] W. Mayer, "Abbildender Radarsensor mit sendeseitig geschalteter Gruppenantenne," Dissertation, Universität Ulm, 2008.

This work was supported by the German Research Foundation (DFG) under the program 'Ultrabreitband-Funktechniken für Kommunikation, Lokalisierung und Sensorik (UKoLoS)' (priority program SPP1202). Website: http://www-emt.tu-ilmenau.de/ukolos/

Mario Leib, Arnold Gronau, and Wolfgang Menzel
Microwave Techniques, University of Ulm
Albert-Einstein-Allee 41, 89081 Ulm
Fax: +49 (0)731/50–26359
E-mail: mario.leib@uni-ulm.de

Bernd Schleicher and Hermann Schumacher
Electron Devices and Circuits, University of Ulm
Albert-Einstein-Allee 45, 89081 Ulm

Eva Schmitt
Now with: Nokia GmbH
Lise-Meitner-Straße 10, 89081 Ulm

Jochen Dederer
Now with: EADS Deutschland GmbH
Wörthstraße 85, 89077 Ulm